frontiers | Frontiers in Remote Sensing

TYPE Original Research
PUBLISHED 23 January 2026
DOI 10.3389/frsen.2026.1723667

OPEN ACCESS

EDITED BY
Shengbiao Wu,
The University of Hong Kong, Hong Kong, SAR China

REVIEWED BY
Bibhuti Bhusan Sahoo,
Centurion University of Technology and Management School of Engineering and Technology, India
Shijie Li,
The University of Hong Kong, Hong Kong, SAR China

*CORRESPONDENCE
Zandile Mncube,
223150281@stu.ukzn.ac.za

RECEIVED 17 October 2025
REVISED 28 December 2025
ACCEPTED 02 January 2026
PUBLISHED 23 January 2026

CITATION
Mncube Z, Xulu S and Mbatha N (2026) Evaluating the efficacy of hybrid deep learning models in assessing temporal night-time light trends for the cities of Cape Town, Durban and Johannesburg in South Africa.
Front. Remote Sens. 7:1723667.
doi: 10.3389/frsen.2026.1723667

Evaluating the efficacy of hybrid deep learning models in assessing temporal night-time light trends for the cities of Cape Town, Durban and Johannesburg in South Africa

Zandile Mncube[1]*, Sifiso Xulu[1,2] and Nkanyiso Mbatha[3]

[1]School of Agricultural, Earth and Environmental Sciences, University of KwaZulu-Natal, Westville Campus, Durban, South Africa, [2]Department of Geography, University of South Africa, Florida Campus, Johannesburg, South Africa, [3]Council for Scientific and Industrial Research, Holistic Climate Change, Smart Places, Pretoria, South Africa

Introduction: Increasing research demonstrates the value of nighttime light (NTL) data for studying human activities, including urban change. The public availability of these products on geospatial computing platforms like Google Earth Engine (GEE) has expanded their use for various applications and adding incorporation of Python and R analysis tools.
Methods: Deep learning techniques such as Wavelet Denoise (WD), Empirical Mode Decomposition (EMD), and Enhanced Empirical Mode Decomposition (EEMD) are seldom used in NTL research, but here were used them with long short-term memory (LSTM) to form hybrid models to denoise and decompose NTL trajectory to interpretable frequency levels and intrinsic mode functions (IMFs) that improve trend evaluation. We leveraged these tools to assess the performance of deep learning models in modelling and forecasting NTL trends in Cape Town, Durban, and Johannesburg from 2014 to 2023. Root mean square error (RMSE) and mean absolute error (MAE) were used to evaluate model performance.
Results: The findings indicate that integrating decomposition approaches with LSTM enhances the precision and interpretability of NTL modelling. In Cape Town, the RMSE for all models varied from 0.083 to 0.114, while the MAE ranged from 0.063 to 0.085. Durban, RMSE ranged from 0.069 to 0.133, and MAE varied from 0.055 to 0.108. Johannesburg, RMSE ranged from 0.124 to 0.449 and MAE varied from 0.102 to 0.383.
Discussion: Because of decomposition advantages, EEMD-LSTM hybrid model showing superior efficacy in Cape Town and Johannesburg, whilst EMD-LSTM model excelled in Durban.
Conclusion: From the findings we can conclude that these models can enhance NTL analysis.

KEYWORDS

deep learning, forecasting, LSTM, nighttime light, NTL trends

1 Introduction

Satellite remote sensing has been used effectively in many cities worldwide to analyze urban dynamics and forecast changes, using multiple sensor platforms, most of which are now publicly available. These sensors include the Visible Infrared Imaging Radiometer Suite (VIIRS) Day/Night Band (DNB), which, after its predecessor Defense Meteorological Satellite Program (DMSP)-Operational Linescan System (OLS) (1992–2013), has been providing nighttime light (NTL) data since 2014 (Elvidge et al., 2013). VIIRS has a clear advantage over DMSP-OLS as it provides better spatial and temporal resolutions leading to fewer errors such as over glow of NTLs in cities (Elvidge et al., 2013). This product has been used in a variety of studies to examine human-caused activities such as urban growth (Zhou et al., 2018), land use land cover changes (Hasan et al., 2019), urban heat islands (Sun et al., 2020b), and population growth (Wang et al., 2020). However, to keep up with these changes, there is a greater demand for high-density observations to enable more timely representation and analysis (Zhu et al., 2019). Note for emphasis that the VIIRS DNB data can be influenced by a number of atmospheric factors which may lead to uncertainties observed while analyzing ground NTL (Wang et al., 2020).

The VIIRS-DNB product is considered suitable for temporal pattern analysis and forecasting of urban dynamics using deep learning models due to its night-time observation capability at monthly intervals. Li et al. (2017) found that VIIRS is more accurate than DMSP-OLS in predicting county-level gross domestic product (GDP). Ivan et al. (2020) estimated Romania's *per capita* income at the local level using VIIRS-DNB NTL data and a machine learning algorithm. Ye et al. (2020) found that persistent cloud cover results in low-quality and missing observations and prevents the VIIRS-DNB time series data from reaching their full potential. Since there was a significant lack of reliable observations, they subsequently proposed prediction of NTL using the spatiotemporal statistical method (STSM). The "forecast" package on the R computing platform was used by Zhao et al. (2020) to analyze and forecast VIIRS DNB NTL image to identify changes and hurricane-related impacts in Puerto Rico. Gu et al. (2022) combined the time series datasets of DMSP/OLS and VIIRS-DNB NTL to model and forecast the GDP of Chinese provinces by examining at the relationships between NTL and GDP. Nevertheless, there is a dearth of studies evaluating the effectiveness of deep learning models in studying NTL trends hence our intention with this work is to address this gap.

The availability of NTL data on public platforms such as the Google Earth Engine (GEE) is an important advance in understanding urban patterns around the world, and studies leveraging these resources have increased (Mncube and Xulu, 2022). GEE is such platform and has been very useful in accessing, managing, analyzing and visualization of petabytes of datasets. These datasets are pre-processed before being made available online, facilitating quick access and eliminating many obstacles related to big data management (Gomes et al., 2020). GEE is a cloud-based platform that offers the JavaScript API and Python API programming languages which makes it feasible for datasets to be downloaded and analyzed in other platforms and software's (Tamiminia et al., 2020).

Recent years have seen a rapid application of deep learning algorithms to big geographic data using high-performance computing and cloud-based platforms such as GEE, which have created unprecedented opportunities to assess NTL dynamics in urban areas (Sun et al., 2020b). For example, Zhang et al. (2021) proposed a novel CNN-based approach in modelling of a relationship between MODIS and the daily Luojia 1-01 NTL data. They proposed a deep learning method based on the ResNet to establish a relationship between the two datasets. However, some deep learning algorithms that require large training datasets are currently unavailable in GEE due to computational limitations, requiring users to run these algorithms outside of this platform (DeLancey et al., 2019). Leung et al. (2019) employed deep learning approaches that included PASCAL Visual Object Classes (VOC) 2007, Faster Region-based Convolutional Neural Network (R-CNN), Visual Geometry Group 16 (VGG16) and Residual Network 10 (ResNet10) algorithms for feature extractions in the low-light environment imageries. Sun et al. (2020a) used deep learning approaches with VIIRS imagery and land cover data to estimate GDP in Contiguous United States United States (CONUS) to estimate Gross Domestic Product (GDP). Ni et al. (2020) applied deep learning approaches in poverty prediction using nighttime and daytime satellite imagery. They utilized VGG-Net, Inception-Net, ResNet and DenseNet algorithms as feature extractors. These studies prove the growing attention paid to using deep learning in NTL applications. Nonetheless, exploring and exploiting GEE capabilities in the combination of deep learning and NTL applications is still inadequate.

Deep learning algorithms are very useful in time series analysis as they are data hungry analysis methods and can effectively manage and analyze big data (Munappy et al., 2022). Mann-Kendal statistical test, Sequential Mann-Kendal (SQMK) test, wavelet denoise, the empirical wavelet transform (EWT), and the empirical mode decomposition (EMD) are the deep learning models that will be utilized in this study. The long short-term memory (LSTM) model is the recommended model for forecasting of future instances hence it is also employed in this study (Mbatha and Bencherif, 2020). These methods as can analyze and learn trends and patterns of big of data making it easy for future prediction to be done (Munappy et al., 2022). They uncover trends and extract useful information about the data. They can also define seasonality and pick up irregular components, or residuals of the data, which is very crucial for forecasting analysis (Torres-Velázquez et al., 2020). EMD and EWT are two signal decomposition techniques that are used to enhance the performance of the hybrid time series forecasting models by breaking down a signal into its smaller components. LSTM is a powerful hybrid deep learning model that has been demonstrated to be a better version of recurrent neural networks (RNNs) that can more effectively learn the information in time series data. It is capable of accurately capturing the variance in time series data. To improve overall accuracy, time series data should first be divided into a number of more predictable components because employing LSTM in its most basic form results in low accuracy hence the combination with the EWT, EMD, and EEMD (Mbatha and Bencherif, 2020).

NTL data may have been recommended by researcher many times, but this does not mean it is perfect. There is a possibility for it to be inconsistent and fractured in the time series record which may limit its utility for temporal urban analysis (Zhang et al., 2024). This is the reason for the reason recommendation of employing deep learning models to better understand the data (Mncube et al., 2024). The usage of hybrid deep learning models over time in research has shown their great capabilities in time series forecasting, making them a prominent tool to use with NTL data (Mahmoud and Mohammed, 2024). Deep

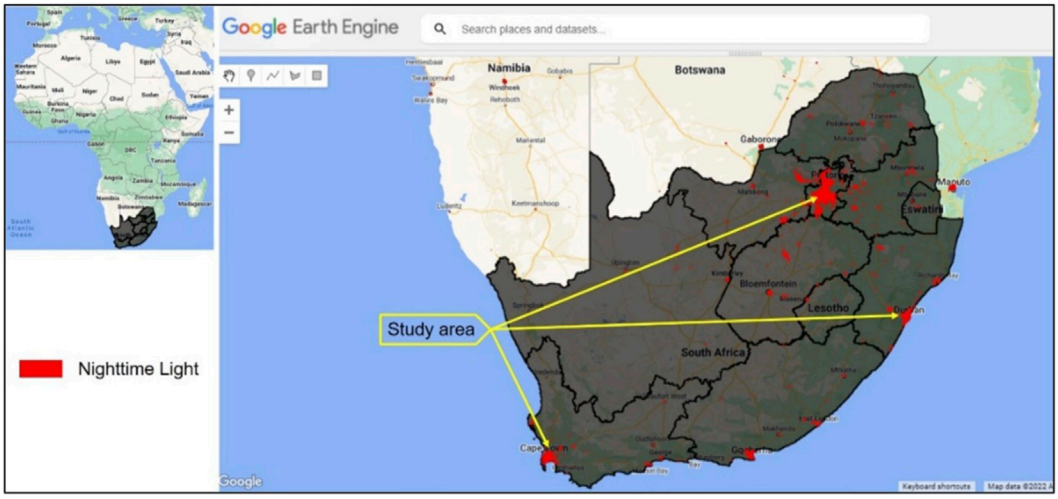

FIGURE 1
Study area (source: Mncube et al., 2024).

learning applications in NTL analysis can be done in different ways using different models. In the present study, we contribute to our previous work (Mncube et al., 2024) by evaluating the efficacy of hybrid deep learning models in analyzing temporal NTL trends for the cities of Cape Town, Durban and Johannesburg.

The rest of the paper is organized as follows: Section 2 comprises the materials and methods, outlining the process and steps undertaken to collect and analyze the data. Sections 3 and 4 are dedicated to the presentation of the results as well as discussion of the findings. Lastly, Section 5 provides the conclusion of the study, summarising the key insights and implications drawn from the research.

2 Materials and methods

2.1 Study area

The three most populous metropolitan municipalities in South Africa—the cities of Cape Town, Durban, and Johannesburg—are test areas for this study. These are shown in Figure 1 below. These cities not only have the highest population but are also known for their economic contribution to the country's economic growth. About 4 M people call the City of Cape Town home, an increase of 2.6% since 2011 (Statistics South Africa, 2022a). The population of the City of Johannesburg is 4.9 M, with a growth rate of 3.2% (Statistics South Africa, 2022b), while the City of Durban is 3.7 M with a growth rate of 2.3% (Statistics South Africa, 2022c). The area of Durban is 2,555 km^2, that of Johannesburg is 1,643 km^2 and the City of Cape Town is 2,441 km^2. As the urban areas of these cities have grown over time, it stands to reason that NTL instances there are likely to change as well. The current changes are related to the urban and economic development that each city experiences over time. In South Africa, 84.4% of people have access to electricity, which they use, in part, for nighttime lighting (World Bank, 2022). In particular, 90.8% of households in Johannesburg, 89.3% in Durban, and 93.7% in the City of Cape Town have access to electricity as a source of lighting (Sovacool et al., 2022).

2.2 Nighttime light

Version 1 of VIIRS DNB NTL data was retrieved from the GEE using a JavaScript code developed from previous work of NTL analysis by Jeswani et al. (2019) for the years 2014–2023. VIIRS DNB NTL data has been recommended as better NTL data source compared to DMSP-OLS because of its qualities such as having an on-board calibration system, offering monthly data instead of annual and the data filtering capabilities (Elvidge et al., 2013). The VIIRS sensor filters the data to ensure that the data affected by cloud cover, lightning, lunar illumination, and fires is excluded from captured data. Several studies have also supported this claim sustaining the superiority of VIIRS over DMSP (Levin et al., 2019; Sahoo et al., 2020; Sun et al., 2020b). This then affirmed the employment of VIIRS DNB NTL data in this study. An Excel spread sheet in a format of.csv was downloaded and imported to the Python environment called Anaconda distribution for time series analysis. The comma-separated values (CSV) Excel spreadsheet downloaded contained average NTL values for the three cities, Cape Town, Durban and Johannesburg. Two columns were found on the spreadsheet, one for the date and the other for the average NTL radiance values. The dataset was split into 80% for training and 20% for testing/validation, this applied to training each pf the deep learning models employed in this study. In the Python environment cleaning and analysis of the data was done using deep learning algorithms as adapted from the work of Mbatha and Bencherif (2020). The algorithms used in this study are further elaborated upon in the following sections.

2.3 Empirical wavelet transform

In this study empirical wavelet transform (EWT) was utilized to extract trends in the NTL time series. EWT is a decomposition method developed by Gilles (2013) that decomposes NTL signals into a collection of amplitude modulated-frequency modulated (AM-FM) signals according to the information contained within

the Fourier spectrum. This algorithm extracts different modes of NTL signal by designing a suitable filter bank suitable for each dataset. When applying the EWT in a time series x_((t)), the process of signal decomposition can be described as follows:

The first step calculates the Fourier spectrum F(ω) of the NTL signal using the fast Fourier transform algorithm while the second step determines the boundaries ω_i by proper segmentation of the Fourier spectrum (Equations 1, 2):

$$\omega_i = \frac{f_i + f_{i+1}}{2} \; for \; 1 \le i \le 1 \tag{1}$$

$$\varphi i(w) = \begin{cases} 1, if \; (1+\gamma)\omega_i \le |\omega| \le (1-\gamma)\omega_{i+1} \\ \cos\left[\frac{\pi}{2}\beta\left(\frac{1}{2\gamma\omega i+1}\left(|\omega| - \left(1-_\gamma\right)\omega_{i+1}\right)\right)\right], \text{if } (1-\gamma)\omega_{i+1} \le |\omega| \le (1+\gamma)\omega_{i+1} \\ \sin\left[\frac{\pi}{2}\beta\left(\frac{1}{2_{\gamma\omega i}}\left(|\omega| - (1-\gamma)\omega_i\right)\right)\right], \text{if } (1-\gamma)\omega_i \le |\omega| \le (1+\gamma)\omega_i \\ 0, \text{Otherwise} \end{cases} \tag{2}$$

where $\{f_i\}, i = 1, 2, \ldots, N$ are the frequencies that correspond to local maxima and $f_0 = 0$. The third step then constructs empirical wavelet $\varphi i(w)$ in the following form (Equation 3):

and

$$\varphi i(w) = \begin{cases} 1, if \; |\omega| \le (1-\gamma)\,\omega_i \\ \cos\left[\frac{\pi}{2}\beta\left(\frac{1}{2\gamma\omega_i}\left(|\omega| - (1-\gamma)\omega_i\right)\right)\right]', \text{if } (1-\gamma)\omega_{i \le |\omega| \le (1+\gamma)} \\ 0, \text{Otherwise} \end{cases} \tag{3}$$

where $\gamma = min_i\left(\frac{\omega_{i+1}-\omega_i}{\omega_{i+1}+\omega_I}\right)$. In both the above equations, the function $\beta(x)$ represents an arbitrary $C^k[0,1]$ function, such that (Equation 4),

$$\beta(x) = \begin{cases} 1, if \; x \ge 1 \\ 0, if \; x \le 0 \end{cases} and \; \beta(x) + \beta(1-x) = 1 \; \forall x \in [0,1] \tag{4}$$

Gilles (2013) and Daubechies (1992) have used the formula as Equation 5:

$$\beta(x) = x^4\left(35 - 84x + 70x^2 - 20x^4\right) \tag{5}$$

The above listed equations are based on the assumption that the Fourier support [0,π] is segmented into N contiguous segments. The frequency ω_i is then denoted to be the limits between each segment.

The fourth step is to calculate the approximate and detail coefficients using the following Equations 6 and 7:

$$W_x(i,t) = \left(x(t), \psi_i(t)\right) = \int x(\tau)\psi_i(\tau - t)d = F^{-1}\left[x(\omega)\psi(\omega)\right] \tag{6}$$

$$W_x(1,t) = \langle x(t), \psi_1(t)\rangle = \int x(\tau)\psi_i(\tau - t)d = F^{-1}\Big[x(\omega)\psi_i(\omega) \tag{7}$$

The final step involves reconstructing the original signal in order to obtain different modes in the following Equation 8 format:

$$x(t) = W_x(1,t) \times \varphi_1(t) + \sum_{i=2}^{N} W_X(i,t) \times \psi_i(t) \tag{8}$$

2.4 Singular spectrum analysis (SSA)

For better understanding of NTL trends, on top of EWT we added the singular spectrum analysis (SSA) which also helps in smoothening the NTL data of the three cities. SSA extracts and analyses trends, signals, trends, and patterns for long time-series datasets. SSA allows for NTL trajectory matrix to be broken down to meaningful and interpretable components shown by eigenvalues (Mbatha and Bencherif, 2020). SSA has five steps of data analysis with different purposes. The first phase, known as the embedding step, creates a lagged version of the time series by converting the NTL time series data into a trajectory matrix. The trajectory matrix is then broken down into single values. The trajectory matrix is broken down into three matrices, U, S, and V^T, by the Singular Value Decomposition (SVD). Where V^T is the right singular vector, S is a diagonal matrix of singular vectors, and U is the left singular vector. Subsequently, the singular values and their accompanying singular vectors are grouped together. In the fourth stage, the grouped singular vectors are used to rebuild the time series data, with each group of singular vectors being assigned a certain time series component. Forecasting or analyzing the time series components that have been reconstructed is the last phase.

2.5 Mann-Kendal

Assessing monotonic trends when assessing time series data is vital before making any projections using any data (Mbatha and Bencherif, 2020). The Mann-Kendal method is often employed to assess these trends and it is defined as a non-parametric and rank-based method mostly utilized to assess monotonic trends in a time series of data (Mbatha and Xulu, 2018). The Mann-Kendall test statistic is calculated from a formula derived from Kendall's study which was later modified by Pohlert (2016) outlined as follows (Equations 9 and 10):

$$S = \sum_{k=1}^{n-1}\sum_{j=k+1}^{n} sgn\left(x_j - x_k\right) \tag{9}$$

where,

$$\text{Sgn} = \begin{cases} +1, if \; x > 1 \\ 0, if \; x = 0 \\ -1, if \; x < 1 \end{cases} \tag{10}$$

The average value of S is $E[S] = 0$, and the variance σ^2 is calculated using the following equation (Equation 11):

$$\sigma^2 = \left\{n(n-1)(2n+5) - \sum_{j=1}^{p} t_j\left(t_j - 1\right)\left(2t_j + 5\right)\right\} \Big/ 18 \tag{11}$$

Where t_j is the number of data points in the jth tied group, and p is the number of the tied group in the time series. Under the assumption of a random and independent time series, the statistical function S is approximately normal distributed given that the below Z-transformation equation (Equation 12) is used:

$$Z = \begin{cases} \frac{S-1}{\sigma}, if \; S > 1 \\ 0, if \; S = 0 \\ \frac{S+1}{\sigma}, if \; S < 1 \end{cases} \tag{12}$$

The value of the statistic S is associated with Kendall's $\tau = S/D$ (Equation 13)

$$D = \left[\frac{1}{2}n(n-1) - \frac{1}{2}\sum_{j=1}^{P} t_j\left(t_j - 1\right)\right] \text{½} \left[\frac{1}{2}n(n-1)\right] \text{½} \quad (13)$$

One issue of the Mann-Kendall is that it is not able to give the complete structure of the whole time series but it very much important for NTL dynamics to be understood and outlined as there might be important changes that need to be noted during the study period. This challenge is resolved by applying the Mann-Kendall test statistic called Sequential Mann-Kendall (SQMK) sequentially to every single period.

2.6 Sequential Mann-Kendall (SQMK) test

The Sequential Mann-Kendall (SQMK) test was first proposed by Sneyers (1991) and is used in identifying any abrupt changes that are present in the long term time series trends. Two time series are produced by this test procedure: a forward/progressive ($u(t)$) and a retrograde/backward ($u'(t)$). Plotting the progressive and retrograde time series in the same figure is necessary in order to maximize the effectiveness of this trend identifying method. If the times series cross each other and diverge at any point in this study ±1.96, that means there is a statistically significant trend. The point where they meet indicates the time period where the trend turning point trend (Mbatha and Xulu, 2018). The SQMK is computed using ranked values of y_i of the given time series $(x_1, x_2, x_3, \ldots, x_n)$ in the analyses. The magnitudes of y_i, $(i = 1, 2, 3, \ldots, n)$ are compared with the y_i, $(j = 1, 2, 3, \ldots, j-1)$. The number of occurrences where $y_i > y_j$ is counted at each comparison and subsequently transferred to ni. The following (Equation 14) therefore defines the statistic t_i:

$$t_i = \sum_{j=1}^{t} n_i \quad (14)$$

The mean and variance of the statistic t_i are given by Equations 15 and 16

$$E(t_i) = \frac{i(i-1)}{4} \quad (15)$$

And

$$Var(t_i) = \frac{i(i-1)(2i-5)}{72} \quad (16)$$

Finally, the sequential values of the statistic $u(t_i)$ which are standardized are calculated using the following (Equation 17):

$$u(t_i) = \frac{t_i - E(t_i)}{\sqrt{Var(t_i)}} \quad (17)$$

The forward sequential statistic, also known as the progressive statistic, is produced using this equation. The same time series $(x_1, x_2, x_3, \ldots, x_n)$ are utilized to compute the backward/retrograde statistic values $(u'(ti))$. However, the computation of the statistic values begins at the end of the time series. When the forward and backward sequential statistics are combined, it is possible to determine the approximate start of a trend. Furthermore, a 95% confidence level was considered in this study, meaning that the critical limit values are ±1.96. This method has been utilized to study trends in subjects like temperature, precipitation, vegetation indices, etc. But it has not been identified in any of the NTL studies. LSTM model was preferred over traditional models like ARIMA because of its ability to learn patterns in the time series dataset and to model and forecast based on both short- and long-term patterns learned.

2.7 Wavelet denoise (WD)

Wavelet-based denoising techniques are the most preferred for denoising neural signals because of their unique ability to reduce noise. Wavelet denoise (WD) breaks down the original NTL time series data into components at different frequencies. The frequency levels can capture both short-term and long-term patterns easier. WD enables the model to effectively capture and analyze complex patterns and noise in the datasets (Halidou et al., 2023). The denoising involved three steps done by the code used in Python, which are denoising, thresholding and reconstruction. The data is denoised by breaking it down to different frequency components and then, based on calculated threshold that is based on the noise level, which is then applied to the wavelet coefficient, this is the stage that removes noises. The reconstruction of denoised data us then data which return the final denoised data that was combined with LSTM. this process has been observed to be important in improving the accuracy of the analysis models used in time series forecasting.

2.8 Empirical mode decomposition

The Empirical mode decomposition (EMD) forms an important part of the Hilbert-Huang transform (HHT). The signal is decomposed into the intrinsic mode functions (IMFs) that include both the trend and finite oscillations that supply information on different scales of the original signal. The EMD method is self-adaptive time-space analysis method. It is designed to process time series data that are non-stationary and non-linear. The EMD decomposes the time series as a finite sum of $N + 1$ IMFs $f_k(t)$, to produce Equation 18:

$$f(t) = \sum_{k=0}^{N} f_k(t). \quad (18)$$

An IMF is an amplitude modulated frequency modulated function, which can be mathematically represented in the following (Equation 19):

$$f_k(t) = F_k(t)\cos\left(\varphi_k(t)\right) where\, F_k(t), \varphi_k'(t) > 0 \forall t. \quad (19)$$

Gilles (2013) assessed the set of equation that make up the EMD method, such that he outlined that f_k and φ'_k vary much slower than φ_k. It should also be noted that the IMF parameter f_k behaves as a harmonic component. These IMFs are extracted by first computing the upper, $f(t)$, and the lower $f\_(t)$, envelopes using a cubic spline interpolation method from the maxima and minima of f. Thereafter,

the mean envelop is calculated using the following formula Equation 20:

$$m(t) = \left(\frac{\bar{f}(t) + \underline{f}(t)}{2} \right) \quad (20)$$

And finally, the IMF candidate is computed as computed as follows (Equation 21):

$$r_1(t) = f(t) - m(t). \quad (21)$$

Under normal conditions, r_1 (t) does not fulfill the properties of an intristic mode function, which is why an acceptable IMF candidate is reached by iterating the same process r_1 and the subsequent r_k. The ultimate retrained IMF is given by Equation 22:

$$f_1(f) = r_n(f) \quad (22)$$

2.9 Enhanced empirical mode decomposition (EEMD)

Enhanced Empirical Mode Decomposition (EEMD) is a data-driven decomposition technique that addressed the limitations that may have been observed while performing the EMD. EEMD improves the decomposition process by incorporating noise-based methods that make it more effective and reliable in handling non-linear and non-stationary signals. The following are the steps followed in performing EEMD.

The first step of the EEMD is the denoising stage where the noise in the signals is removed. This is done using Equation 23:

$$x_i(t) = x(t) + w_i(t) \quad (23)$$

Where $x(t)$ is the original signal, $w_i(t)$ is the noise sequence, and $x_i(t)$ is the noise-added signal.

The second step is the application of EMD on each of the noise-added signal to decompose it into IMFs (Equation 24).

$$x_i(t) = \sum_{j=1}^{m} IMF_{ij}(t) + r_i(t) \quad (24)$$

where $IMF_{ij}(t)$ are the IMFs obtained from the noise-added signal, $r_i(t)$ is the residual and m is the number of IMFs.

The third step follows in performing the ensemble averaging where the corresponding IMFs' ensemble average are computed across all decompositions to obtain the final IMFs (Equation 25).

$$IMF_j(t) = \frac{1}{N} \sum_{i=1}^{N} IMF_{ij}(t) \quad (25)$$

Where N is the total number of noise-added signals.

Finally, the signal reconstruction is performed. The original signal can be reconstructed using the ensemble averaged IMFs (Equation 26).

$$x(t) = \sum_{j=1}^{m} IMF_j(t) + r(t) \quad (26)$$

Where $r(t)$ is the residual.

2.10 Long short-term memory (LSTM)

The LSTM is a type of recurrent neural network (RNN) proposed by Hochreiter and Schmidhuber (1997) that are often used together with deep learning. RNNs are deep learning networks of improved multilayer perception (Mbatha and Bencherif, 2020). Traditional artificial neural networks (ANNs) mostly employ the usage of feedforward neural network while the RNNs are referred to as the recurrent network because in their processing, they receive input, use that information to update the hidden states occurring depending on the previous computations and make predictions based on each element in a sequential format. These are said to have memory because they store information about the processes the network underwent. They outlined the mathematical form of the structure displayed above as the following equations (Equations 27–32):

$$f_t = S\left(W_F \cdot \left[\hat{y}_{t-1,} x_t\right] + b_f\right) \quad (27)$$

$$i_t = S\left(W_I \cdot \left[\hat{y}_{t-1}, x_t\right] + b_i\right) \quad (28)$$

$$\hat{C}_t = \tanh\left(W_C \cdot \left[\hat{y}_{t-1}, x_t\right] + b_c\right) \quad (29)$$

$$C = f_t \cdot C_{t-1} + i_t \cdot \hat{C}_t \quad (30)$$

$$o_t = S\left(W_o \cdot \left[\hat{y}_{t-1}, x_t\right] + b_o\right) \quad (31)$$

$$\hat{y}_t = o_t \cdot \tanh C_t \quad (32)$$

In this study we trained the LSTMs with the following architecture: an LSTM layer and a fully connected layer of the decomposition matrices. We established a flexible learning rate depending on the model performance. We used between 50 and 100 epochs and a batch size equaling to 1. Lastly, a different number of hidden units were evaluated through the best cross-validation error using the "adam" optimizer.

Four LSTM neural networks-based data-driven time series forecasting models namely, LSTM, WD-LSTM, EMD-LSTM and EEMD-LSTM were utilized in this study and the details of their architectural designs are alluded to in the sections to follow.

2.11 Model design

The Mann-Kendal and the SQMK statistic test investigates significant backward or forward trends to be noted in the dataset before it can be used for analysis. The WD denoises data to improve the accuracy of the prediction and also overcome any issues relating to long-term dependencies forecasting problems. The EMD-LSTM developed algorithm is compared to the EEMD-LSTM. The two algorithms are also compared to the LSTM model in terms of forecasting of NTL trajectories. The LSTM utilized in this study is a Python LSTM system ran in the Google Collab interface.

Figure 2 shows the details of the procedure followed in the analysis conduction in this study. The decomposition of the NTL time series data into moderately stable IMFs and one residual item occurs in the first stage using the EMD approach. The LSTM neural network is used to forecast each normalized IMF, including the residual, in the following phase. The third stage involves reverse-normalizing the LSTM neural network's forecasting findings before aggregating them through summation to produce the final anticipated outcomes. To forecast all of the IMFs and the

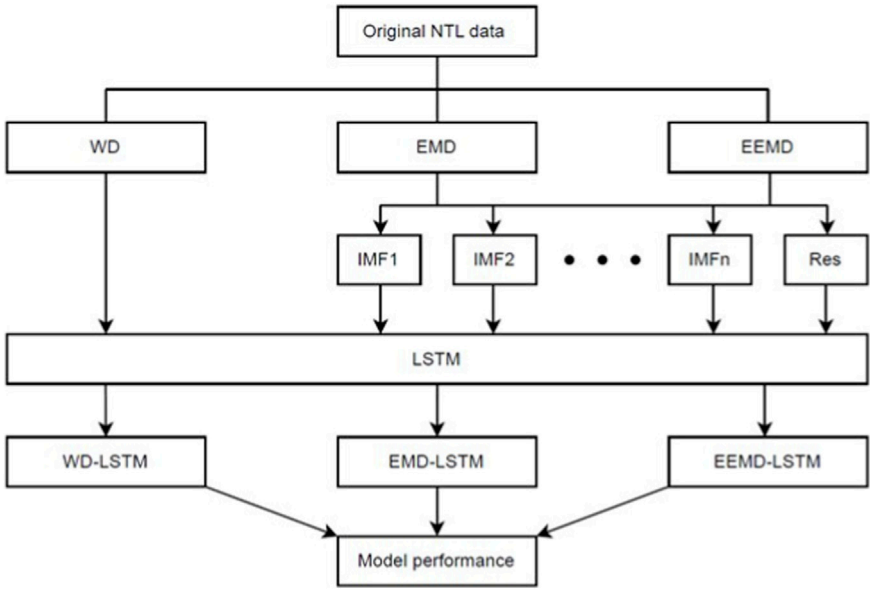

FIGURE 2
Deep learning model design.

residue, the trained LSTM models are fed the testing dataset as input. After each modelling is done, the performance of each model is evaluated utilizing the Taylor Diagram. Taylor (2001) presented a graph that summarizes numerous perspectives of model performance, including correlation, root-mean-square difference, and variance ratio. The regular starting step in approving models of natural phenomena is to decide whether their behavior takes after the observed pattern. Typically, plots showing that a pattern of observed performance is reproduced by the model and is displayed as evidence of its effectiveness.

2.12 Model performance

Generally, there is no standard method for evaluating a model's forecasting abilities (Mbatha and Bencherif, 2020). By employing common performance measures, which are shown by equations below the model performance in this study is evaluated by comparing the predicted values with the corresponding observed NTL values. This was done using a Taylor diagram which is a graphical presentation that is used to assess how the models perform. It visualizes the accuracy and precision of each model through assessing the radical distance of each model against original observations which shows the standard deviation of each prediction. There was also computation of different statistics such as standard deviation, root mean square error (RSME), correlation coefficient, mean absolute error (MAE), etc. Which were calculated for the predicted values against the original observations. Both RMSE and MAE identify the difference between the predicted values and the actual values of NTL. The smaller the difference shown by these two evaluations the better the performance of the models. Researchers have debated between the superiority of either RMSE or MSE, other have recommended MSE while others say RMSE is better. For this reason, it was best to use both RMSE and MSE for better judgement (Chai and Draxler, 2014).

The formulae for the comparison statistics that were used in this study which are the MAE and the RMSE are shown by Equation 33 and Equation 34 below. The correlation coefficient and standard deviation are to be presented graphically in the results section of this paper.

$$MAE = \frac{1}{N}\sum_{j=1}^{N}\left|p^{j}_{estimated} - p^{j}_{real}\right| \tag{33}$$

$$RMSE = \sqrt{\frac{1}{N}\sum_{j=1}^{N}\left(p^{j}_{estimated} - p^{j}_{real}\right)} \tag{34}$$

3 Results

3.1 Nighttime light data time series and trends

This study focused on evaluating the efficacy of deep learning models in analyzing changes and trends in NTL radiance values through performance analysis of the models. Therefore, before any thorough trend analysis can be done, it is important to first understand the original sense of the data. Figures 3a–c depicts the time series plot for the three cities under study over the period of 2014–2023. The city of Cape Town shows a rise and fall trend. The city of Durban on the other side depicts an escarpment-like pattern with downward trend noticeable after its peak in 2017 which make it show a wave-like trend pattern. Lastly, the city of Johannesburg is somewhat showing the opposite of Durban with a steady fluctuation noticed in some years, but

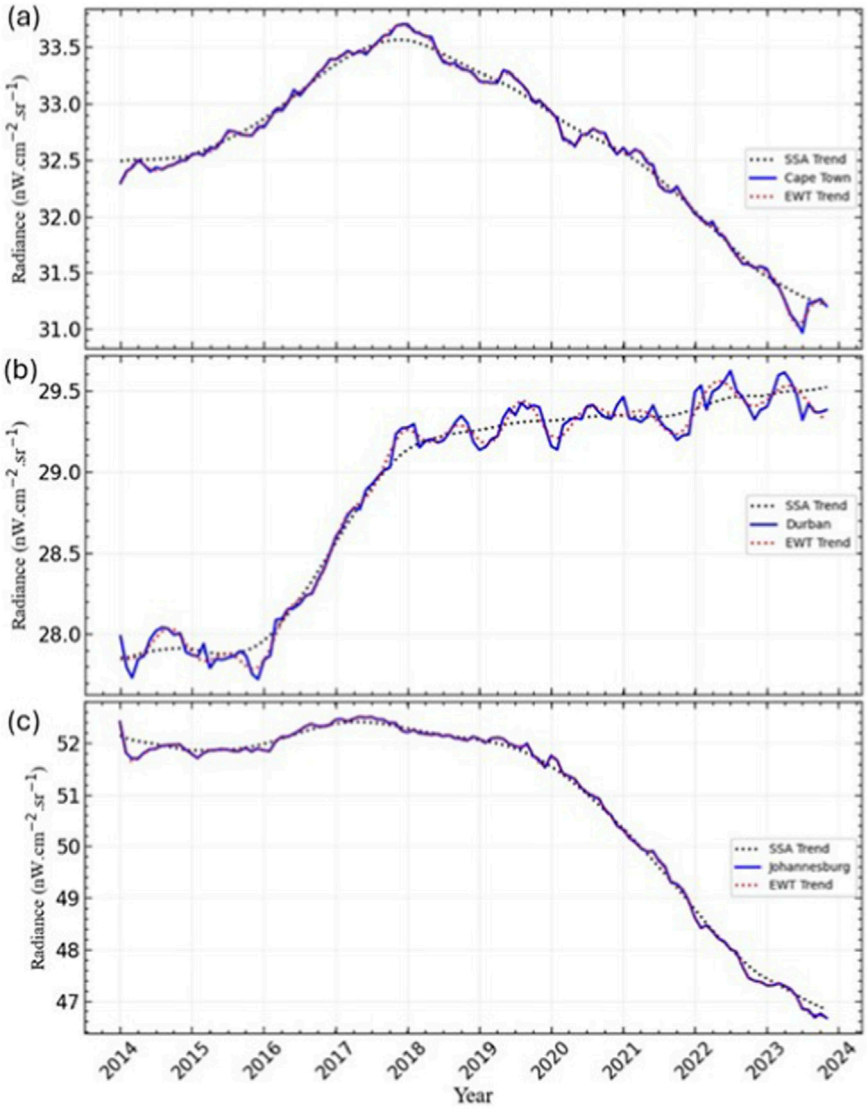

FIGURE 3
NTL time series for cities of **(a)** Cape Town, **(b)** Durban, and **(c)** Johannesburg.

for the rest of the period after that a significant decline is observed.

3.2 Mann-Kendall and SQMK statistic tests results

The Mann-Kendal statistic test uses the z-score to determine the significance of the trends. The z-score limits for the current study under Mann-Kendall were −1.96 to 1.96 with the p-value limit being 0.05. The z-score shows the significance of the discovered trend. A positive z-score shows an increasing trend, and a negative z-score shows a decreasing trend in the time series. It ranges between −1.96 and 1.96, any value more or less than this range indicates a significant trend.

The z-scores for the three cities are as follows: Cape Town is −5.4641, Durban is 11.748 and Johannesburg is −9.2515, with p-values; 4.653×10^{-8}, 2.2×10^{-16}, and 2.2×10^{-16}, respectively. Additionally, Kendall tau values were also computed and were as follows; -3.390555×10^{-1}, 7.290346×10^{-1} and -5.739316×10^{-1}, respectively. In this case from both z-score and the Kendal tau values we can see that only Durban showed a significant increase trend while both Cape Town and Johannesburg showed significant decreasing trends over time. Moreover, low p-value indicates strong evidence suggesting a significant trend while a high p-value indicates weak evidence suggesting no significant trend. We can therefore conclude that the NTL trends observed from the three cities show significant trends as the values are all lower than 0.05.

Subsequently, the SQMK test revealed the results shown in Figure 4 below. The SQMK reveals hidden trends and points of change for each trend. From the graphs below we can see that the trend changes are mainly significant in all the three cities. Also, there are no point where the progressive and the retrograde meet, this

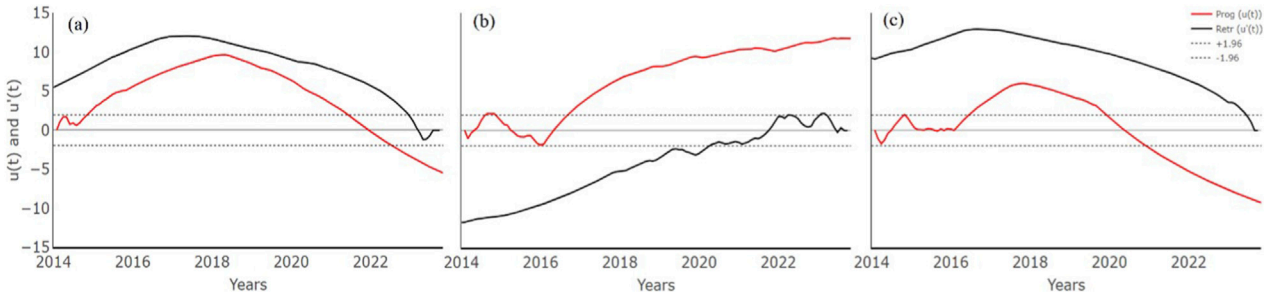

FIGURE 4
NTL trend changes extracted by SQMK for **(a)** Cape Town, **(b)** Durban, and **(c)** Johannesburg.

makes it difficult to tell the points where the changes in trends occur. Nonetheless, whether increasing or decreasing, the trends are definitely significant.

3.3 LSTM models forecasting

After analyzing the surface trends of the NTL data in Section 3.1, we proceeded to develop and execute the LSTM model for comprehensive evaluation of NTL performance. To prepare for the model development, we employed three robust techniques: WD, EMD, and EEMD, to decompose the non-stationary and non-linear signals from the NTL time series data. The EMD and EEMD methods divided the original data series into multiple moderately stable intrinsic mode functions (IMFs) and one residual component. The rationale for executing both EMD and EEMD was to enhance the efficacy of the LSTM model.

The EMD and EEMD methods were applied to the original data, yielding IMFs and residual components. The number of IMFs generated and analyzed varied according to the dataset for each city. The IMFs derived from the EMD and EEMD procedures show three aspects. The IMFs generated from the lowest to middle segments of the NTL data for each city denote low frequencies. Secondly, the latter portion of the IMFs signifies elevated frequencies, whereas the residual components illustrate the pattern of NTL throughout the cities.

All sub-band signals obtained from WD, EMD, and EEMD were utilized in the decomposition and denoising phase of the hybrid LSTM model. A hybrid model incorporating deconstructed and denoised data through several techniques was established as the final phase of data analysis. This resulted in hybrids such as WD-LSTM, EMD-LSTM, and EEMD-LSTM. The efficacy of these models was evaluated in comparison to the original NTL data. Prior to evaluating model performance or conducting statistical comparisons, it was necessary to generate the graphical representation of the LSTM models. These are illustrated in Figure 5 below. The figure illustrates the models' performance based on their proximity to the original data trends. The expected and displayed data samples pertain to the most recent years, specifically 2021 to 2023. This arises from the organization and refinement of the established model and data processing. All models for the City of Cape Town have been observed to anticipate values closely aligned with the original NTL data. A similar observation is noted for the city of Durban.

3.4 Model performance

The Taylor diagram (Taylor, 2001) was utilized provides a concise statistical summary of the degree of correspondence between the forecasted NTL patterns and observed NTL patterns. The correlation coefficient and the RMSE differences between the two fields, in conjunction with the ratio of the standard deviations of the two patterns, are all shown by a single point of each model on the displayed a 2–dimensional plot shown above. Together, these insights give a quick outline of the degree of pattern correspondence, allowing one to gage how precisely a model simulates the observed trends. This diagram was particularly valuable in evaluating the relative merits of the competing LSTM models and in checking in general performance as each model advances. In Figure 6 the performance of the models is depicted. The assumption is that the closer the model symbol is the original observation the lesser the standard deviation meaning that the prediction done by the model is high in accuracy. From the representation we can observe that the models performed best for the cities of Cape Town and Johannesburg and poor performance was noticed for the city of Durban. Different factors such as the city structure, economic development and activities, and different social factors, may be accountable for the poor performance of the models in Durban (Han et al., 2022). These factors may have affected the NTL measurement over time. Again, a growth of NTL was only noted in Durban while Cape Town and Johannesburg showed a decline over the year, also affecting the data structure. This may then result in the parameters used in the structuring of the models to not be suitable for generalization for the trends and changes such as those existing in the Durban NTL dataset.

Furthermore, Table 1 below list the statistical values of the assessed statistics to determine how the models performed, which are RMSE and MAE. The RMSE and MAE values are measured in the units as the NTL which is in $nW.cm^{-2}.sr^{-1}$.

For the model to be of good performance, there must be no extremely large outliers existing in its forecasting. This will be shown by the difference existing between the computed values. For Cape Town, the RMSE for all models ranged from 0.083 to

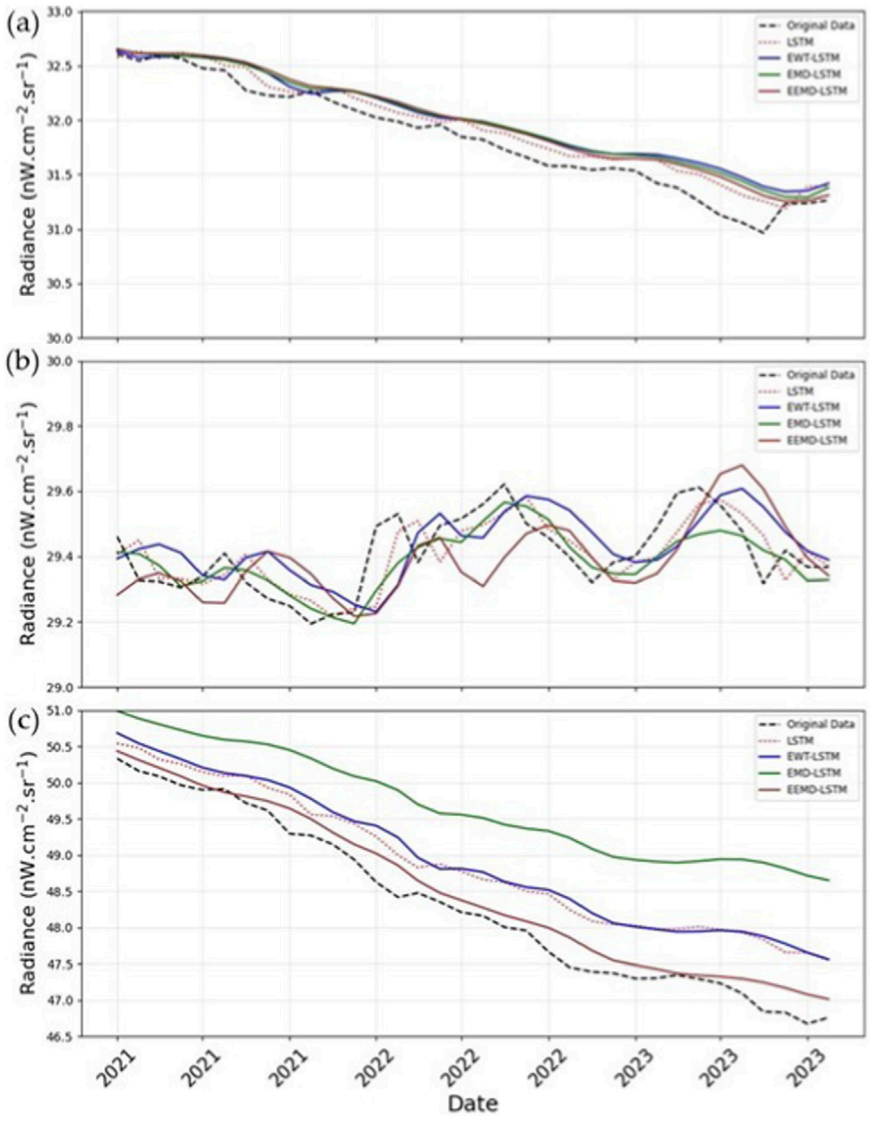

FIGURE 5
LSTM Model plots for **(a)** Cape Town, **(b)** Durban, and **(c)** Johannesburg.

0.114 and MAE ranged from 0.063 to 0.085. For Durban, the RMSE for all models ranged from 0.069 to 0.133 and MAE ranged from 0.055 to 0.108. Lastly, for Johannesburg, the RMSE for all models ranged from 0.124 to 0.449 and MAE ranged from 0.102 to 0.383. Overall, the EEMD-LSTM hybrid models was found to have performed best in the cities of Cape Town and Johannesburg while for the city of Durban it was the EMD-LSTM that had the lowest RMSE and MAE. Similar findings were discovered from the Johannesburg's dataset. However, it is important to note that in Cape Town the original non-hybrid LSTM performed best the EEMD-LSTM followed. Looking at the specificities for each city, from the Cape Town dataset, the RMSE the model with the highest difference was the WD-LSTM and the lowest was from the LSTM. From the city of Durban dataset, both the highest and lowest RMSE and MAE differences were found from the EEMD-LSTM and EMD-LSTM, respectively. These statistics mean that the model with lowest RMSE and MAE differences is making small errors and is most likely performing well. This closeness of the values also suggests that there are no large outliers. If the RMSE were to be much higher than MAE, then that would indicate that a few predictions have large errors.

4 Discussion

These characteristics and trends indicate the presence of various periodicies that affect NTL such as load shedding, economic activities and developments, atmospheric errors and so on. Mainly, atmospheric errors have been noted in several studies as factors that affect the accuracy and quality of the NTL data captured. Key factors such as airglow, light pollution, atmospheric scattering by different things such as aerosols and particulate matter in the atmosphere are the most prominent recorded factors that may affect the capturing of NTL (Uprety

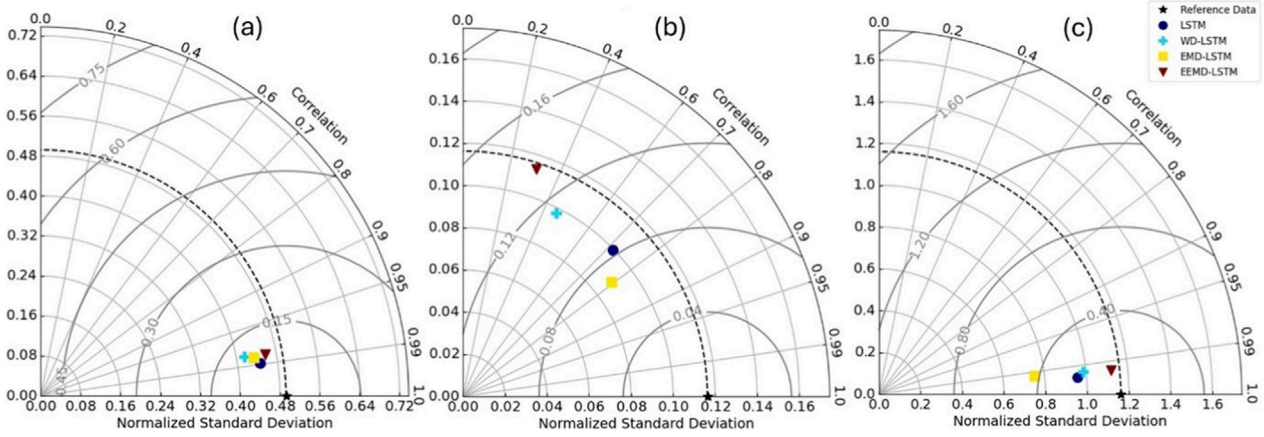

FIGURE 6
Taylor diagram graphical representation of four predictive models developed for forecasting of NTL in **(a)** Cape Town, **(b)** Durban, and **(c)** Johannesburg from 2014 to 2023.

TABLE 1 LSTM hybrid models performance.

Cities	LSTM		WD-LSTM		EMD-LSTM		EEMD-LSTM	
	RMSE	MAE	RMSE	MAE	RMSE	MAE	RMSE	MAE
Cape Town	0.083	0.063	0.114	0.085	0.101	0.079	0.092	0.075
Durban	0.081	0.065	0.111	0.089	0.069	0.055	0.133	0.108
Johannesburg	0.233	0.196	0.223	0.185	0.449	0.383	0.124	0.102

et al., 2017; Wang et al., 2020; Sanchez de Miguel et al., 2020; Zhang et al., 2023).

The Mann-Kendall and SQMK tests help in revealing the underlying trends in the dataset. In this case these tests have revealed and emphasized on the changes in NTL trends occurring in similar patterns as the load shedding occurrence changes in the country. In this case, the Mann-Kendall test revealed that all the changes in the NTL trends were significant based on the values observed. On the other hand, the exact turning points of the trends could not be pinpointed from the SQMK however, the significance once again was clearly visible from the graphs above. The SQMK method unveiled the changes of trend directions in both single and aggregate time series. This helped to identify the associations between the NTL changes, regional dynamics such as load shedding events that may affect the observed changes in NTL.

Several comparison statistics can be utilized to assess the performance of the LSTM models. Shown in the table above are two of those many; RMSE and MAE. To deduce the performance of the model, each hybrid LSTM model was measured against the original NTL dataset for the same dataset of each city. Hodson (2022) reviewed the uses of the RMSE and MAE detailing when they can and cannot be used. His review supported their use in the case of this study as he alluded that each of these statistics are good depending on their application. Most commonly, the association between these two statistics and their relevance in model performance is that their values determine the level of accuracy based on how big or small they are against the target variable (Wang and Lu, 2018).

In the context of this study the EMD-LSTM and EEMD-LSTM performing better than the WD-LSTM model may be due to the added functions to their composition. These include the frequency of decomposition, noise reduction, enhanced feature extraction and how they handled non-stationary NTL data from each city's dataset. These models are able to decompose the time series data to meaningful components to capture both long-term and short-term dependencies. The combination of these then leads to a better forecasting model performance. To sum up, from Table 1 we can deduce that the difference between the predicted values and the original NTL values varied with just a range of 0.05–0.4 which means that the computed evaluation statistics found very little differences between the original NTL data and the predicted values. Both RMSE and MAE for all models was below 0.5. This therefore affirms the good performance of the hybrid models in predicting NTL.

In summary, having the deep learning models perform well in forecasting NTL datasets from these cities prove that VIIRS DNB NTL data is good quality data that may be used in different fields of research. The models proved that the dataset is able to pick up strong temporal patterns over the years. The good performance also means that the data has sufficient historical information that joins into current standing of data. LSTMs used in this study are data-hungry and require recording of even long-term changes in the dataset hence the use of the years 2014–2023. From this we can regard NTL

data as a valuable and appropriate data source that offers a stability through its monthly resolution and can be used in research in the South African context. It is important to mention that the models employed in this study can be improved continuously by refining them, transforming datasets, and using different statistics in their structuring (Munappy et al., 2022). This can improve the results obtained in modelling datasets.

5 Conclusion

Our comparative study examined the performance of deep learning models in predicting NTL patterns in three largest cities in South Africa with the aim of assessing whether the models are efficient in studying NTL patterns or not. The analyses focused on two statistical tests and decomposition techniques were used to develop hybrid LSTM models that thoroughly assessed NTL trends over the years. From the NTL trend analyzed, the City of Cape Town showed a rise and fall pattern with a noticeable decrease towards the end of the study period. The pattern in Durban and Johannesburg was opposite, with Durban showing a steady increase and Johannesburg showing a steady decline. The hybrid LSTM forecasting models revealed that the trend patterns noticed from the datasets from each city were all significant based on the statistical tests studied on them. The performance of these models was also observed to have performed very well with high accuracy. The models showed very few irregularities and no extremely large outliers. The VIIRS DNB datasets showed a possible applicability of their qualities in the geodata science applications and explorations.

The valuable qualities of NTL data revealed through this study make us see that the VIIRS DNB NTL data source is a sustainable data source that can be used in studying urban changes and human activities. This opens for broader research projects that can explore the usability of NTL data in South African region, as a developing country with statistical data challenges. The next project to this one will look at the changes in the cities under study, especially assessing the built-up area against NTL, in order to understand how each of them have been evolving over the years, linking both temporal and spatial changes not just by NTL but in integration with other datasets as well. This will also allow for the exploration of the socio-economic variables that affect the observed NTL patterns.

Data availability statement

Publicly available datasets were analyzed in this study. This data can be found here: https://eogdata.mines.edu/products/vnl/#monthly.

Author contributions

ZM: Writing – original draft, Investigation, Formal Analysis, Data curation, Conceptualization, Project administration, Writing – review and editing, Methodology. SX: Formal Analysis, Writing – original draft, Methodology, Conceptualization, Investigation, Writing – review and editing, Supervision. NM: Writing – review and editing, Methodology, Supervision, Investigation.

Funding

The author(s) declared that financial support was not received for this work and/or its publication.

Acknowledgements

We would like to appreciate the University of KwaZulu Natal for their support in the conduction of this research.

Conflict of interest

The author(s) declared that this work was conducted in the absence of any commercial or financial relationships that could be construed as a potential conflict of interest.

Generative AI statement

The author(s) declared that generative AI was not used in the creation of this manuscript.

Any alternative text (alt text) provided alongside figures in this article has been generated by Frontiers with the support of artificial intelligence and reasonable efforts have been made to ensure accuracy, including review by the authors wherever possible. If you identify any issues, please contact us.

Publisher's note

References

Chai, T., and Draxler, R. R. (2014). Root mean square error (RMSE) or mean absolute error (MAE)? Arguments against avoiding RMSE in the literature. *Geosci. Model Dev.* 7 (3), 1247–1250. doi:10.5194/gmd-7-1247-2014

Daubechies, I., and Heil, C. (1992). Ten lectures on wavelets. *Soc. Industrial Appl. Math.* 6, 697. doi:10.1137/1035160

DeLancey, E., Kariyeva, R. J., Bried, J. T., and Hird, J. N. (2019). Large-scale probabilistic identification of boreal peatlands using google Earth engine, open-access satellite data, and machine learning. *PLoS ONE* 14 (6), e0218165. doi:10.1371/journal.pone.0218165

Elvidge, C. D., Baugh, K. E., Zhizhin, M., and Hsu, F.-C. (2013). Why VIIRS data are superior to DMSP for mapping nighttime lights. *Proc. Asia-Pacific Adv. Netw.* 35 (0), 62. doi:10.7125/APAN.35.7

Gilles, J. (2013). Empirical wavelet transform. *IEEE Trans. Signal Process.* 61 (16), 3999–4010. doi:10.1109/TSP.2013.2265222

Gomes, V. C., G, R. Q., and Ferreira, K. R. (2020). An overview of platforms for big Earth observation data management and analysis. *Remote Sens.* 12 (8), 1253. doi:10.3390/rs12081253

Gu, Y., Shao, Z., Huang, X., and Cai, B. (2022). GDP forecasting model for china's provinces using nighttime light remote sensing data. *Remote Sens.* 14 (15), 3671. doi:10.3390/rs14153671

Halidou, A., Mohamadou, Y., Ari, A. A. A., and Zacko, E. J. G. (2023). Review of wavelet denoising algorithms. *Multimedia Tools Appl.* 82 (27), 41539–41569. doi:10.1007/s11042-023-15127-0

Han, G., Zhou, T., Sun, Y., and Zhu, S. (2022). The relationship between night-time light and socioeconomic factors in China and India. *PLoS ONE* 17 (1), e0262503. doi:10.1371/journal.pone.0262503

Hasan, S., Shi, W., Zhu, X., and Abbas, S. (2019). Monitoring of land use/land cover and socioeconomic changes in south China over the last three decades using landsat and nighttime light data. *Remote Sens.* 11 (14), 1658. doi:10.3390/rs11141658

Hochreiter, S., and Schmidhuber, J. (1997). Long short-term memory. *Neural Comput.* 9 (8), 1735–1780. doi:10.1162/neco.1997.9.8.1735

Hodson, T. O. (2022). Root mean square error (RMSE) or mean absolute error (MAE): when to use them or not. *Geosci. Model Dev. Discuss.* 2022, 1–10. doi:10.5194/gmd-15-5481-2022

Ivan, K., Holobâcă, I., Benedek, J., and Török, I. (2020). VIIRS nighttime light data for income estimation at local level. *Remote Sens.* 12 (18), 2950. doi:10.3390/rs12182950

Jeswani, R., Kulshrestha, A., Gupta, P. K., and Srivastav, S. (2019). Evaluation of the consistency of DMSP-OLS and SNPP-VIIRS night-time light datasets. *J. Geomate* 13, 98–105.

Leung, H. K., Chen, X.-Z., Yu, C.-W., Liang, H.-Y., Wu, J.-Y., and Chen, Y.-L. (2019). A deep-learning-based vehicle detection approach for insufficient and nighttime illumination conditions. *Appl. Sci.* 9 (22), 4769. doi:10.3390/app9224769

Levin, N., Kyba, C., and Zhang, Q. (2019). Remote sensing of night Lights—beyond DMSP. *Remote Sens.* 11 (12), 1472. doi:10.3390/rs11121472

Li, X., Elvidge, C., Zhou, Y., Cao, C., and Warner, T. (2017). Remote sensing of night-time light. *Int. J. Remote Sens.* 38 (21), 5855–5859. doi:10.1080/01431161.2017.1351784

Mahmoud, A., and Mohammed, A. (2024). Leveraging hybrid deep learning models for enhanced multivariate time series forecasting. *Neural Process. Lett.* 56, 223. doi:10.1007/s11063-024-11656-3

Mbatha, N., and Bencherif, H. (2020). Time series analysis and forecasting using a novel hybrid LSTM data-driven model based on empirical wavelet transform applied to total column of ozone at Buenos Aires, Argentina (1966–2017). *Atmosphere* 11 (5), 457. doi:10.3390/atmos11050457

Mbatha, N., and Xulu, S. (2018). Time series analysis of MODIS-derived NDVI for the Hluhluwe-Imfolozi Park, South Africa: impact of recent intense drought. *Climate* 6 (4), 95. doi:10.3390/cli6040095

Mncube, Z., and Xulu, S. (2022). Progress of nighttime light applications within the Google Earth engine cloud platform. *Geocarto Int.* 38, 1–22. doi:10.1080/10106049.2022.2120550

Mncube, Z., Xulu, S., and Mbatha, N. (2024). Analysis of nighttime lights over the cities of cape town, Durban and Johannesburg, South Africa. *Evol. Earth* 2, 100046. doi:10.1016/j.eve.2024.100046

Munappy, A. R., Bosch, J., Olsson, H. H., Arpteg, A., and Brinne, B. (2022). Data management for production quality deep learning models: challenges and solutions. *J. Syst. Softw.* 191, 111359. doi:10.1016/j.jss.2022.111359

Ni, Y., Ye, Y., Li, Y., Li, C., and Chu, D. (2020). An investigation on deep learning approaches to combining nighttime and daytime satellite imagery for poverty prediction. *IEEE Geoscience Remote Sens. Lett.* 18 (9), 1545–1549. doi:10.1109/LGRS.2020.3006019

Pohlert, T. (2016). *Non-parametric trend tests and change-point detection*. Creative Commons License. doi:10.13140/RG.2.1.2633.4243

Sahoo, S., Gupta, P. K., and Srivastav, S. K. (2020). Comparative analysis between VIIRS-DNB and DMSP-OLS night-time light data to estimate electric power consumption in Uttar Pradesh, India. *Int. J. Remote Sens.* 41 (7), 2565–2580. doi:10.1080/01431161.2019.1693077

Sanchez de Miguel, A., Kyba, C., Zamorano, J., Gallego, J., and Gaston, K. J. (2020). The nature of the diffuse light near cities detected in nighttime satellite imagery. *Sci. Rep.* 10 (1), 1–16. doi:10.1038/s41598-020-64673-2

Sneyers, R. (1991). *On the statistical analysis of series of observations*. Geneva: World Meteorological Organization. Available online at: https://www.cabidigitallibrary.org/doi/full/10.5555/19912451385.

Sovacool, B. K., Daniels, C., and AbdulRafiu, A. (2022). Transitioning to electrified, automated and shared mobility in an African context: a comparative review of Johannesburg, Kigali, Lagos and Nairobi. *J. Transp. Geogr.* 98, 103256. doi:10.1016/j.jtrangeo.2021.103256

Statistics South Africa. (2022a). City of cape town. Available online at: https://www.statssa.gov.za/?page_id=993&id=city-of-cape-town-municipality.

Statistics South Africa. (2022b). City of Johannesburg. Available online at: https://www.statssa.gov.za/?page_id=993&id=city-of-johannesburg-municipality.

Statistics South Africa. (2022c). Ethekwini. Available online at: https://www.statssa.gov.za/?page_id=993&id=ethekwini-municipality.

Sun, J., Di, L., Sun, Z., Wang, J., and Wu, Y. (2020a). Estimation of GDP using deep learning with NPP-VIIRS imagery and land cover data at the county level in CONUS. *IEEE J. Sel. Top. Appl. Earth Observations Remote Sens.* 13, 1400–1415. doi:10.1109/JSTARS.2020.2983331

Sun, Y., Wang, S., and Wang, Y. (2020b). Estimating local-scale urban heat Island intensity using nighttime light satellite imageries. *Sustain. Cities Soc.* 57, 102125. doi:10.1016/j.scs.2020.102125

Tamiminia, H., Salehi, B., Mahdianpari, M., Quackenbush, L., Adeli, S., and Brisco, B. (2020). Google Earth engine for Geo-Big data applications: a meta-analysis and systematic review. *ISPRS J. Photogrammetry Remote Sens.* 164, 152–170. doi:10.1016/j.isprsjprs.2020.04.001

Taylor, K. E. (2001). Summarizing multiple aspects of model performance in a single diagram. *J. Geophys. Res. Atmos.* 106 (D7), 7183–7192. doi:10.1029/2000JD900719

Torres-Velázquez, M., Chen, W.-J., Li, X., and McMillan, A. B. (2020). Application and construction of deep learning networks in medical imaging. *IEEE Trans. Radiat. Plasma Med. Sci.* 5 (2), 137–159. doi:10.1109/TRPMS.2020.3030611

Uprety, S., Cao, C., Gu, Y., and Shao, X. (2017). "Improving the low light radiance calibration of S-NPP VIIRS Day/Night band in the NOAA operations," in *2017 IEEE international geoscience and remote sensing symposium (IGARSS)* (IEEE), 4726–4729. doi:10.1109/IGARSS.2017.8128057

Wang, W., and Lu, Y. (2018). Analysis of the mean absolute error (MAE) and the root mean square error (RMSE) in assessing rounding model. *IOP Conf. Series Mater. Sci. Engi.* 324, 012049. doi:10.1088/1757-899X/324/1/012049

Wang, C., Chen, Z., Yang, C., Li, Q., Wu, Q., Wu, J., et al. (2020). Analyzing parcel-level relationships between Luojia 1-01 nighttime light intensity and artificial surface features across Shanghai, China: a comparison with NPP-VIIRS data. *Int. J. Appl. Earth Observation Geoinformation* 85, 101989. doi:10.1016/j.jag.2019.101989

Wang, X., Mu, X., and Yan, G. (2020). Quantitative analysis of aerosol influence on Suomi-NPP VIIRS nighttime light in China. *IEEE J. Sel. Top. Appl. Earth Observations Remote Sens.* 13, 3557–3568. doi:10.1109/JSTARS.2020.3003480

World Bank. (2022). Overview. Available online at: https://www.worldbank.org/en/country/southafrica/overview.

Ye, Y., Deng, J., Huang, L., Zheng, Q., Wang, K., Tong, C., et al. (2020). Modeling and prediction of NPP-VIIRS nighttime light imagery based on spatiotemporal statistical method. *IEEE Trans. Geoscience Remote Sens.* 59 (6), 4934–4946. doi:10.1109/TGRS.2020.3011695

Zhang, L., Ren, Z., Dong, R., Xu, B., and Fu, H. (2021). "Monitoring daily nighttime light based on modis and deep learning: a Belgium case study," in *2021 IEEE international geoscience and remote sensing symposium IGARSS* (IEEE), 5032–5035. doi:10.1109/IGARSS47720.2021.9554903

Zhang, J., Reid, J. S., Miller, S. D., Román, M., Wang, Z., Spurr, R. J., et al. (2023). Sensitivity studies of nighttime top-of-atmosphere radiances from artificial light sources using a 3-D radiative transfer model for nighttime aerosol retrievals. *Atmos. Meas. Tech.* 16 (10), 2531–2546. doi:10.5194/amt-16-2531-2023

Zhang, L., Dong, R., Yuan, S., Zhang, J., Chen, M., Zheng, J., et al. (2024). Deeplight: reconstructing high-resolution observations of nighttime light with multi-modal remote sensing data. *arXiv Preprint arXiv:2402.15659*. doi:10.48550/arXiv.2402.15659

Zhao, N., Liu, Y., Hsu, F.-C., Samson, E. L., Letu, H., Liang, D., et al. (2020). Time series analysis of VIIRS-DNB nighttime lights imagery for change detection in urban areas: a case study of devastation in Puerto Rico from hurricanes Irma and maria. *Appl. Geogr.* 120, 102222. doi:10.1016/j.apgeog.2020.102222

Zhou, Y., Li, X., Asrar, G. R., Smith, S. J., and Imhoff, M. (2018). A global record of annual urban dynamics (1992–2013) from nighttime lights. *Remote Sens. Environ.* 219, 206–220. doi:10.1016/j.rse.2018.10.015

Zhu, Z., Zhou, Y., Seto, K. C., Stokes, E. C., Deng, C., Pickett, S. T., et al. (2019). Understanding an urbanizing planet: strategic directions for remote sensing. *Remote Sens. Environ.* 228, 164–182. doi:10.1016/j.rse.2019.04.020